UNIVERSITY OF OSLO

DEPARTMENT OF PHYSICS

REPORT SERIES

The Performance of the DELPHI SAT Tracker during 1991 and its Contribution to the Absolute Luminosity Measurement

L. Bugge, T. Buran, A.L. Read, and E. Wilhelmsen

Department of Physics
University of Oslo, P.O.Box 1048 Blindern
N-0316 Oslo 3, Norway

UiO/PHYS/94-01
ISSN-0332-5571

Received: 1994-01-19
NIP-94-01

The Performance of the DELPHI SAT Tracker during 1991 and its Contribution to the Absolute Luminosity Measurement

L. Bugge, T. Buran, A. L. Read, and E. Wilhelmsen

Department of Physics, University of Oslo
Postboks 1048, Blindern
N-0316 Oslo, Norway

January 18, 1994

Abstract

The performance of the DELPHI Small Angle Tagger (SAT) tracker in 1991 is presented. A method to use the SAT tracker for monitoring the internal geometry of the SAT calorimeter and thereby improving the luminosity measurement for DELPHI is described. A reduction from 0.35% to 0.05% in the relevant contribution to the systematic error on the luminosity is reported.

1 Introduction

The measurement of the decay width of the Z^0 into invisible final states is used to determine the number of light neutrino species and in addition to set limits on various extensions to the Standard Model. Luminosity measurements made with the DELPHI Small Angle Tagger (SAT) provide the absolute normalization of the hadronic and leptonic cross-sections used to extract the invisible width of the Z^0. The uncertainty in the invisible width is currently dominated by the systematic uncertainty in the luminosity measurement.

The luminosity measurement consists of counting the number of events due to small angle Bhabha scattering ($e^+e^- \rightarrow e^+e^-(\gamma)$) into a precisely known geometric acceptance and dividing by the theoretical cross-section into this acceptance. The SAT detector consists of a pair of calorimeters which surround the beam-pipe at ± 2.3 m from the interaction point, a set of precise acceptance masks located in front of one of the calorimeters and a 2-plane silicon track detector located in front of the calorimeter which is opposite the masks.

Due to the steeply rising, $\sim 1/\theta^3$, angular distribution of Bhabha scattering, the inner radius of the SAT acceptance region must be known with an accuracy of ~ 130 μm to keep its contribution to the systematic uncertainty below 0.2%; this is accomplished with the acceptance masks. In order to achieve a total experimental uncertainty below 0.5%, the other borders of the acceptance region must be known with a precision significantly better than 1 mm, a performance that is not possible with the calorimeter alone.

In this paper we present results of the analysis of the silicon tracker data taken with DELPHI during the 1991 LEP data-taking. A 0.35% contribution to the systematic uncertainty due to geometrical uncertainties is reduced to 0.05%. This result is included in the update of the electroweak parameters paper under preparation by Superteam I [1].

2 Detector Description

The SAT calorimeters are installed on either side of the interaction point and cover scattering angles between approximately 43 and 135 mrad. The segmentation for one half barrel is shown in figure 1. The inner six rings have radial extensions of 3.00 cm and the two outermost 3.25 cm. The first ring starts at a radius of 10 cm, and the Φ segmentation is 15.0 and 7.5 degrees in the inner and outer four rings, respectively. A set of lead masks were installed in front of one of the calorimeters (side "C" of the DELPHI detector) to define a precise acceptance region. More detailed descriptions of the calorimeter can be found in references [2] and [3].

A SAT tracker unit of 2 planes was installed in front of the SAT calorimeter on side A, opposite the masked calorimeter in arm C. Planes "1" and "3" are located

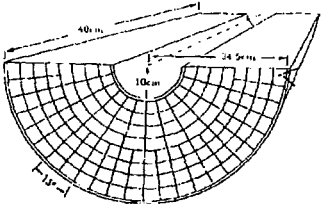

Figure 1: Half a section of one SAT calorimeter, consisting of 144 logical readout elements [6].

at $z = -230.0$ and -202.7 cm and cover about 2096 and 1480 cm^2, respectively. The sensitive region extends from 43.3 to 120.3 mrad, and the inner radii of both planes are 9.95 cm. The planes are composed of 3 rings of 300 μm thick silicon-strip detectors with 47 radial strips per detector. Plane 1 has an additional fourth ring of detectors with 39 radial strips per detector. Each detector covers a 5° azimuthal sector and is mounted on a fan-shaped Kevlar printed circuit board together with its front-end readout electronics. A section of a fan is shown in figure 3. A set of 72 fans gives a full 2π azimuthal coverage for one plane, as shown in figure 4. There is a one strip radial overlap between detectors, and an overlap of 300±50 μm ($\sim 0.15°$) in Φ. The resolution in Φ has been improved by rotating the planes $\pm(5/3)°$, respectively. The fans are supported by a rigid Kevlar structure which is hung from the front face of the SAT calorimeter. For a cross sectional view of the tracker, see figure 2.

The front-end readout electronics for the tracker is a VLSI circuit implemented in CMOS called "Balder" [1]. Each Balder chip contains charge amplifiers and discriminators for 48 channels of silicon-strip detectors. The digital outputs of the discriminators are latched into a register and the encoded addresses of channels above threshold are read out through a serial data bus. The discriminator threshold is controlled by an externally applied voltage.

A more detailed technical description of the SAT tracker can be found in reference [5].

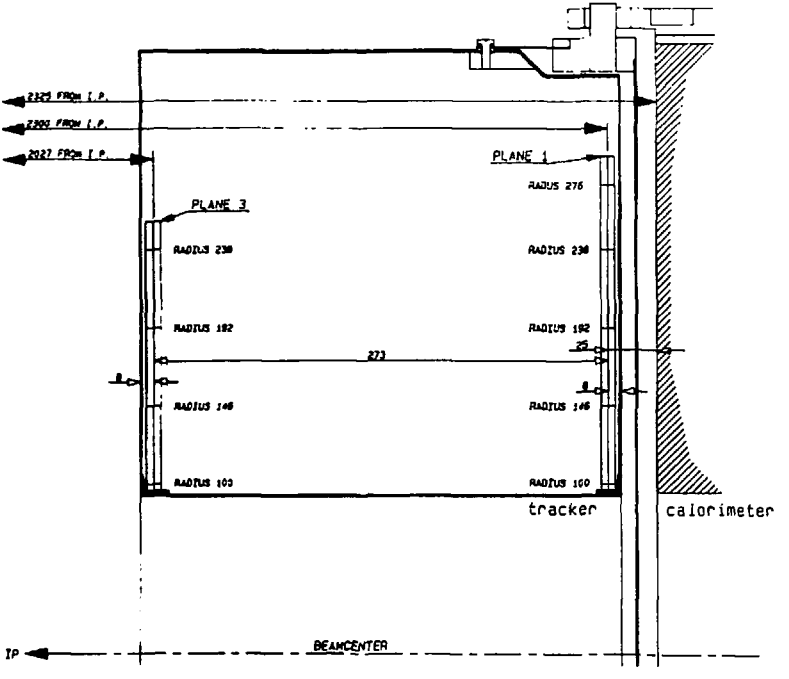

Figure 2: A cross sectional view of the SAT detector installed on the A-side of DELPHI. The dimensions are given in units of mm. The interaction point (IP) is to the left.

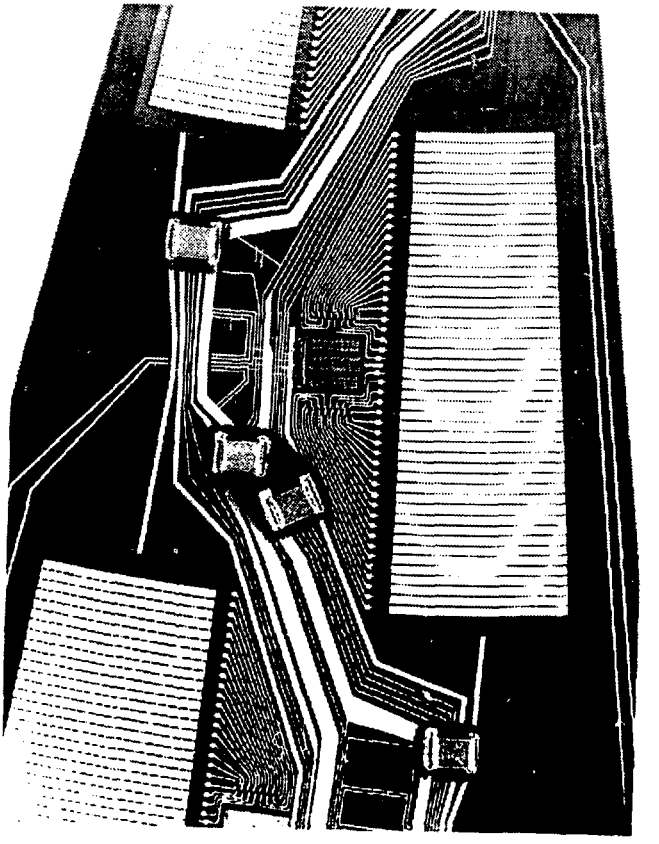

Figure 4 A view of part of a fan-shaped kevlar printed circuit board, showing the layout of Babber readout chips and silicon strip detectors.

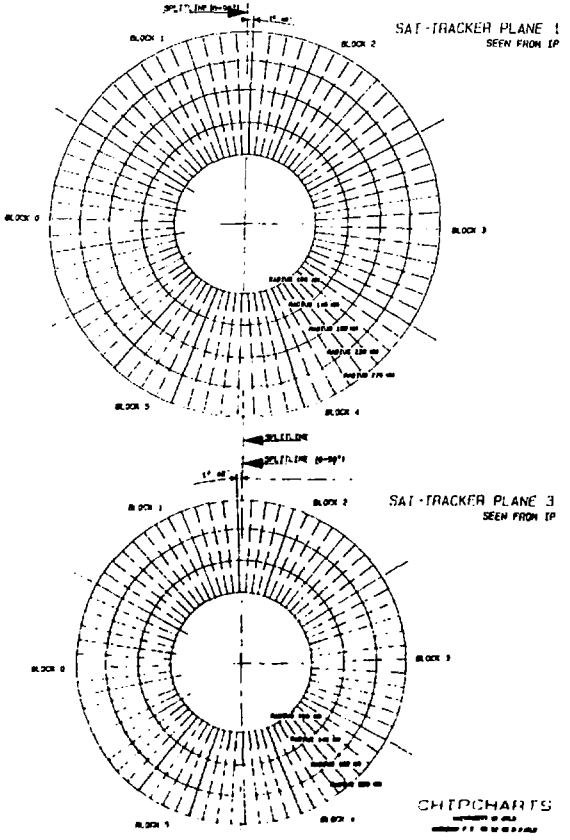

Figure 4: Geometry of the SVI tracker planes, seen from the interaction point (IP).

3 Analysis of the 1991 data

3.1 Event and track selection

Under normal conditions the tracker data would be sampled for each beam crossing and the results latched until they are either read out after positive first and second level trigger decisions, or reset due to negative first or second level decisions. To avoid serious noise problems in the two outer rings of plane 1 and in the outermost ring of plane 3 when sampling each beam crossing, the tracker was sampled every 4^{th} or 5^{th} beam crossing. A bit stored in the SAT trigger data indicates whether the tracker was active for a given beam crossing.

A simple centre-of-gravity (COG) method was used to reconstruct the radial and azimuthal coordinates (R_{cal}, Φ_{cal}) of electromagnetic showers in the calorimeter:

$$R_{cal} = \sum_{i=1}^{M} E_i r_i / \sum_{i=1}^{M} E_i, \qquad \Phi_{cal} = \sum_{i=1}^{M} E_i \phi_i / \sum_{i=1}^{M} E_i, \tag{1}$$

where E_i, ϕ_i and r_i are the energy and the azimuthal and radial coordinates of readout elements in the reconstructed shower. A shower is defined as a cluster of M neighboring elements with individual energy depositions at least 3 standard deviations above the pedestal.

A sample of 48719 reconstructed events has been studied in the following analysis, each event fulfilling the criteria of a Bhabha event as described in reference [3], which basically requires a single high energy shower in each calorimeter within the geometrical acceptance region. In order to avoid edge effects, the projection of R_{cal} to the relevant tracker plane was required to be more than 1.5 cm inside the edges of the active area of the tracker.

To reduce the tracker data volume, only active strips found inside an (R,Φ) window of (6 cm x 24°) in each plane were recorded in data summary files during the processing of the raw data for further analysis. This "search" window was centered in each plane about the interpolated line between the impact point measured by the calorimeter and the interaction point. To be able to measure the background in the detector, active strips in a randomly selected 5° sector outside the search window (the "background" window) were also recorded. When measuring detection efficiencies and background rates, a more restrictive "signal" window of 3 cm x 20° was desired.

The signal of Bhabha events in the tracker is clearly seen in figures 5 and 6. Figure 5 shows the radius of strips in the signal window of plane 1 versus the radius of strips in the signal window of plane 3 (projected along the line to the interaction point on to plane 1) for the selected events with at least one active strip in the signal windows of both planes. Figure 6 shows the corresponding measurements of the Φ coordinates. The points away from the dense signal region along $R_1 = R_3$ are mainly due to random noise in events for which the tracker was inefficient.

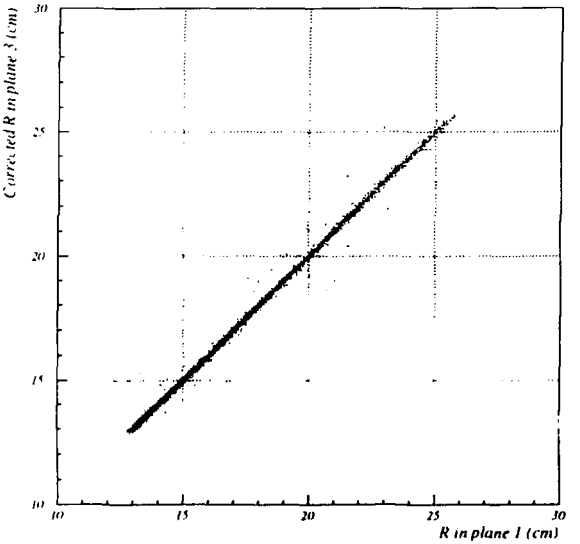

Figure 5 Radius in plane 3 (projected on to plane 1) versus plane 1 for selected Bhabha events.

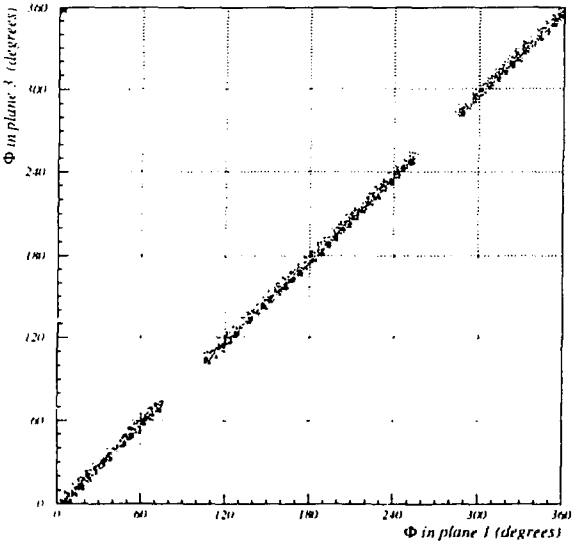

Figure 6. Φ in plane 3 versus Φ in plane 1 for selected Bhabha events. The serated pattern is due to the 5° segmentation and 2·(5/3)° rotation of the silicon strips. The zones of low activity around 90° and 270° are caused by the "butterfly" lead mask in arm C which rejects Bhabha events in these regions.

Threshold (mV)	Bias voltage (V)	Noise Plane 1 (%)	Noise Plane 3 (%)
320	25	0.20±0.02	0.19±0.02
280	25	0.70±0.23	< 0.17
320	35	0.27±0.05	0.11±0.03
280	35	0.40±0.10	0.34±0.09

Table 1: The probability per event for one or more strips in the signal window to fire randomly for various discriminator thresholds and detector bias voltages, measured in randomly selected 5° sectors outside the signal window in Bhabha events.

3.2 Noise studies

A small sample of Balder chips has a hit frequency well above the Bhabha signal as shown in figure 7. This activity is due to 182 noisy strips (0.8% of the total) which are later suppressed from further analysis. Figure 8 shows that after suppressing the noisy strips, the Φ distribution of fired strips in the background window is still peaked at Φ_{cal}. The fired strips in the peak are obviously associated with the Bhabha event, hence a 25° cut is used to exclude them when estimating the random noise background. After the cut both planes have roughly uniform noise distributions.

The probability of one or more strips to fire randomly in the signal window, as calculated from the background data, is shown in table 1 for various operating conditions. The detectors are expected to be fully depleted with a bias voltage of 25 V. A discriminator threshold setting of 300 mV corresponds to about half the mean signal expected from a minimum ionizing particle. The background has a clear dependence on both the detector bias voltage and the discriminator threshold.

The complete absence of signals in some regions was used to identify dead Balder chips. About 5% of the total detector area was found to be inactive.

The probability of one or more strips in the signal window to fire randomly, averaged over the various operating conditions used during the year, is 0.20 ± 0.04% and 0.16 ± 0.04% for planes 1 and 3, respectively. The average probability of a given strip to fire is $2 \cdot 10^{-5}$ per event. The probability of finding two or more active strips in the signal window is 18.1 ± 0.2% for plane 1, and 15.3 ± 0.2% for plane 3. Figure 9 shows the distributions of the total number of hits per event in *each plane*. *The expected sources of this multiple activity and their individual* contributions to the total are the following:

- Random noise contributes less than 0.2%.
- The 0.15° overlap in Φ is measured to contribute 1.1 ± 0.1% and 1.7 ± 0.1% for planes 1 and 3, respectively.

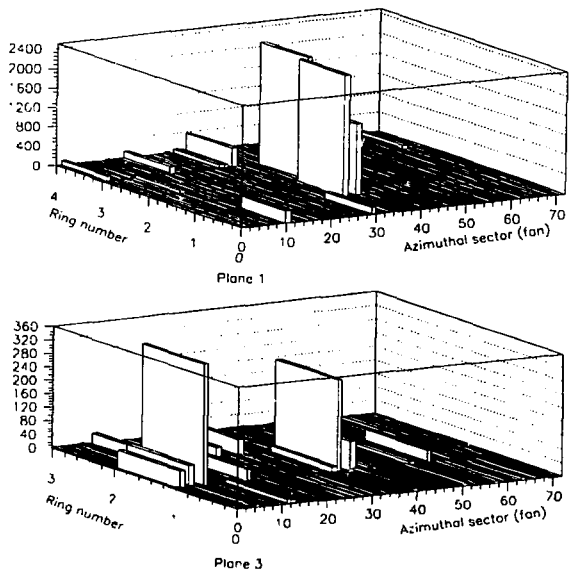

Figure 7: Random noise distribution in the tracker.

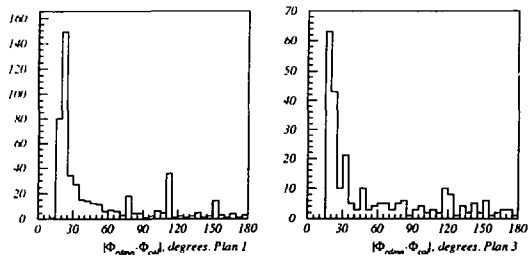

Figure 8: The difference in Φ between active strips in the background window and the reconstructed shower in the calorimeter for Bhabha events in planes 1 and 3.

- The overlap in R is measured to contribute $1.79 \pm 0.06\%$ and $1.43 \pm 0.06\%$ for planes 1 and 3, respectively.
- Simulations made with EGS4 [7] indicate that the rate of back-scattered particles from the calorimeter is less than 1% [9].
- Pair production in the beam-pipe contributes about 4% according to EGS4 simulations [10].

To try to identify additional sources of events with extra hits in the signal window, the difference in R of strips with the same Φ as the strip in the reconstructed track was plotted as shown in figure 10. Events with 10 or more hits in the signal window were ignored and the overlapping strips at the inner and outermost edge at each detector were suppressed. The fraction of events with an adjacent strip active is $3.73 \pm 0.09\%$ and $4.01 \pm 0.09\%$ for planes 1 and 3, respectively. This strong peak indicates a problem with cross-talk on the signal lines between a Balder readout chip and its corresponding silicon detector. Cross-talk on the readout chip itself is ruled out because neighboring silicon strips are not bonded to neighboring readout channels. The wide, asymmetric tails are characteristic of interactions with the detector. Very soft electrons are trapped in the magnetic field and drift parallel to the beam direction, thus appearing preferentially at smaller radii than the primary electron. Neither of these effects were taken into account in the detector simulation used for this analysis.

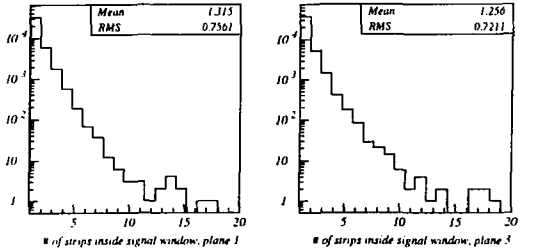

Figure 9: Number of active strips in the signal windows in planes and 3.

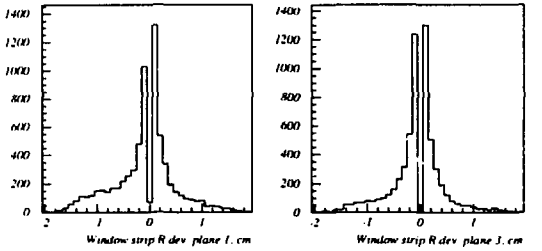

Figure 10: Difference in radius between the strip in the reconstructed track and nearby strips with the same Φ coordinate for planes 1 and 3.

Threshold (mV)	Bias voltage (V)	ϵ_1, Plane 1 (%)	ϵ_3, Plane 3 (%)	ϵ_{13} (%)
320	25	90.2±0.2	89.6±0.2	1.5±0.1
280	25	93.3±0.9	92.3±0.9	0.7±0.3
320	35	93.7±0.3	90.5±0.3	1.2±0.1
280	35	96.8±0.4	94.3±0.5	0.7±0.2

Table 2: The efficiency of the tracker planes for different discriminator thresholds and bias voltages and the 2-plane correlated inefficiency, ϵ_{13}. The data are corrected for known dead areas and regions disabled due to noise suppression.

3.3 Efficiency studies

The efficiency for plane k is $\epsilon_k = \frac{N_a}{N_t}$, where N_a is the number of events with one or more strips active inside the signal window, and N_t is the total number of reconstructed Bhabha events in the calorimeter with the tracker active and with a shower position within the acceptance of the tracker plane in question. Results of a study with different discriminator thresholds and detector bias voltages are shown in table 2. Optimized efficiencies of 96.8±0.4% for plane 1 and 94.3±0.5% for plane 3 were found after correcting for known dead and noisy (filtered out) areas of the detector.

The two-plane inefficiency, i.e. no hits in either plane in the signal window, was *measured* to be $\epsilon_{13} = 0.7 \pm 0.2\%$. The fact that ϵ_{13} differs from the product $(1-\epsilon_1)\cdot(1-\epsilon_3) = 0.18\%$ is evidence of the presence of correlated effects. Such effects may come from a hard bremsstrahlung in the beam-pipe resulting in a hard photon passing through the tracker planes without interacting, while the soft electron is bent out of the tracker acceptance window by the magnetic field. In ref. [11] the frequency of such events was estimated with a Monte Carlo simulation to be of the order 1%. Assuming that the only two sources of both planes being inefficient are the correlated inefficiency from hard scattering and the combination of each plane's statistical inefficiency, the probability of correlated inefficiency p_c can be measured, as well as the true plane efficiencies ϵ_1^T, ϵ_3^T (corrected for the correlated effects inherent in ϵ_1, ϵ_3). Defining the corrected and uncorrected single plane inefficiencies $p_k^T = 1 - \epsilon_k^T$, $p_k = 1 - \epsilon_k$, $k = 1, 3$, one has $\epsilon_{13} = p_c + (1 - p_c)p_1^T p_3^T$, or, in terms of the uncorrected inefficiencies: $\epsilon_{13} = p_c + (p_1 - p_c)(p_3 - p_c)/(1 - p_c)$. Solving this equation with $\epsilon_{13} = 0.007$ one finds $p_c = 0.56\%$, in rough agreement with the simulation. After correcting for the correlated inefficiency using the relations $p_k^T = (p_k - p_c)/(1 - p_c)$, $k = 1, 3$, the plane efficiencies rise to $\epsilon_1^T = 97.3\%$ and $\epsilon_3^T = 94.8\%$.

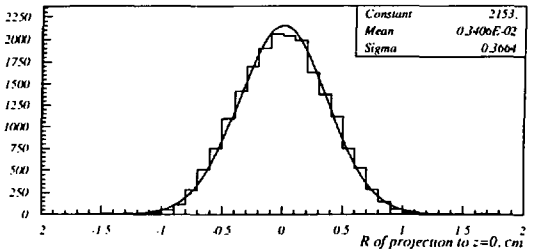

Figure 11: The miss distance in the r-z plane at the interaction point of unambiguous tracks found in Bhabha events.

3.4 Impact parameter resolution

The impact parameter or miss-distance in the r-z plane at the nominal interaction point was measured in events that contained exactly one active strip inside the signal window of each plane. The expected resolution of the impact parameter is 0.365 cm [8]. The measured resolution is 0.366 ± 0.002 cm, as seen in figure 11. One 60° sector was suppressed from this analysis due to a hardware failure that caused the least significant bit in the address of all strips in that sector of one plane to be stuck on. A software correction to this corrupted data allowed an unbiased recovery of the radial position information, but with somewhat poorer resolution.

The good agreement between the expected and measured miss-distance resolution indicates that the spread of the radial detector positions is less than about 100 μm. This is consistent with the combined effects of the expected precision of the internal support and alignment structure and the precision with which individual detector positions on a Kevlar printed circuit board (a fan) are known. Due to a mistake during the construction of the fans, the position of each detector with respect to a ceramic alignment tab located at the end of each fan had to be measured afterwards. The position corrections were as large as 700 μm in the worst case.

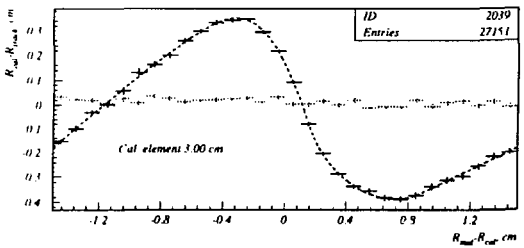

Figure 12: The points with solid error bars show the radial S-curve effect for calorimeter elements with radial extension 3.00 cm. The points with dashed error bars show the data corrected with a spline function fitted to the raw data (the dashed curve).

3.5 The S-curve effect

Due to the crude COG method used for the position reconstruction in the calorimeter, the shower coordinates are systematically distorted. These distortions, known as the S curve effect[9, 12], are illustrated in figures 12 and 13 for the R and Φ coordinates, respectively. The (R_{cal}, Φ_{cal}) coordinates in the figures give the position of the shower reconstructed in the calorimeter, (R_{mid}, Φ_{mid}) is the position of the center of the calorimeter element, and $(R_{track}, \Phi_{track})$ is the impact point determined by the tracker. Only events with exactly one active strip inside the signal window of each plane were plotted.

The S-curves have been fitted to polynomial spline functions and the resulting functions (see appendix A) were used to correct the data. The corrected differences between the calorimeter and tracker measurements of the shower impact coordinates are shown in figures 12 and 13. The distribution of impact radii in the calorimeter before and after correcting for the S-curve are shown in figure 14. The corrected data follow the $\sim 1/R^3$ behavior expected from Bhabha scattering. The S-curve correction has reduced the RMS of the difference between impact radii reconstructed with the calorimeter and tracker by a factor two, as shown in figure 15. After subtracting the theoretical contribution of the tracker to the resolution of the radial impact point, the radius resolution of the corrected calorimeter is observed to be 1.5 mm.

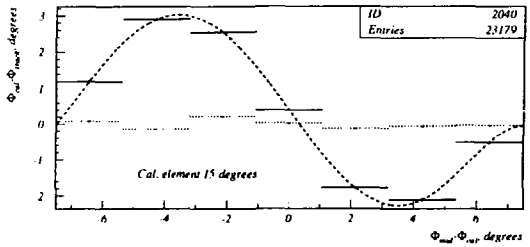

Figure 13: The azimuthal (Φ) S-curve effect for calorimeter elements with an opening angle of 15 degrees. The points with solid error bars show the raw data. The points with dashed error bars show the data corrected with a spline function fitted to the raw data (the dashed curve).

4 Improved luminosity measurement

Two facts have prevented a direct, event-by-event use of the SAT tracker information in the luminosity measurement: The tracker planes are only 90–95% efficient, and the sampling and readout rate was downscaled to avoid serious electronic noise problems. Therefore an indirect use of the SAT tracker has been developed. The basic idea is to survey the geometry of the SAT calorimeter with a sample of events which have an unambiguous response in the tracker. An unambiguous response means that one and only one strip was found in the signal window of each of the two planes. In this way the calorimetric radial cuts can be understood to a precision given by the tracker geometry, rather than by the rough calorimeter geometry. Furthermore, the analysis becomes independent of the downscaled readout and tracker plane efficiencies.

4.1 Measurement of acceptance corrections

Given a total of N_t events with unambiguous tracker response, they can be divided into four non overlapping classes based on whether or not the events pass the cuts that *define the acceptance* of the calorimeter or tracker as follows:

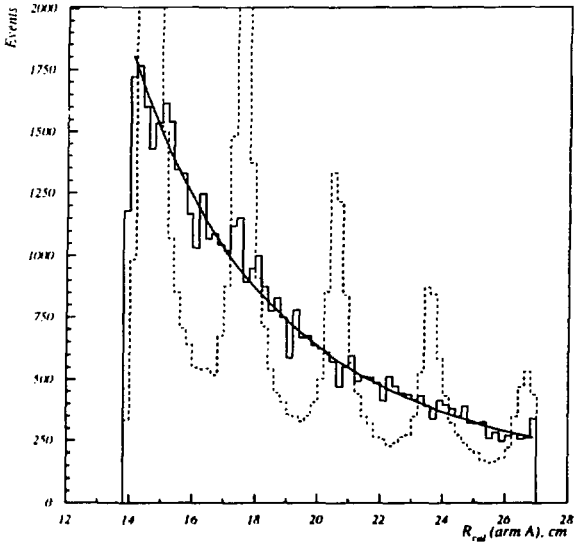

Figure 14: The dashed and solid lines show the reconstructed radius R_{cal} in calorimeter A before and after the S-curve correction measured with the tracker, respectively. The solid curve shows the result of a fit of R^{-3} to the corrected data between 14 and 27 cm.

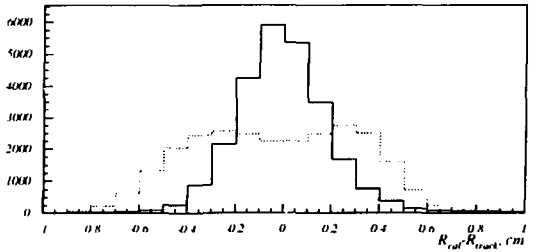

Figure 15: The difference in measured radius between calorimeter A and the tracker, $R_{cal} - R_{track}$ *before (dashed) and after (solid) the S-curve correction.*

CT:	Calorimeter cut	.and.	Tracker cut
$C\overline{T}$:	Calorimeter cut	.and.	.not. Tracker cut
$\overline{C}T$:	.not. Calorimeter cut	.and.	Tracker cut
$\overline{C}\overline{T}$:	.not. Calorimeter cut	.and.	.not. Tracker cut

The total number of events is

$$N_t = N_{CT} + N_{C\overline{T}} + N_{\overline{C}T} + N_{\overline{C}\overline{T}}$$

The numbers of events accepted by the tracker cuts and by the calorimeter cuts are, respectively:

$$N_T = N_{CT} + N_{\overline{C}T}$$

$$N_C = N_{CT} + N_{C\overline{T}}$$

Thus the corrected number of Bhabha events corresponding to the number of events within the acceptance defined by the tracker, N_T, is

$$N_T = N_C(1 + \frac{N_{\overline{C}T} - N_{C\overline{T}}}{N_C})$$

The relative correction $C = \frac{N_{\overline{C}T} - N_{C\overline{T}}}{N_C}$ is also to be applied to the number of Bhabha events accepted by the calorimeter cuts when measuring the luminosity from the full data sample (ignoring the tracker information). The statistical error in the correction factor C appears as a systematic uncertainty in the luminosity

and is calculated from multinomial statistics, neglecting the small covariance terms.

Corrections to the previous, *calorimeter-only luminosity measurement [3]* (hereafter referred to as the "standard" method), were determined for the two residual radial acceptance borders (the lead ring in front of calorimeter C providing the primary definition of the crucial inner radial acceptance border):

1. The border at small radius in calorimeter A in the shadow of the lead mask. In the standard analysis the selection criterion is $R_A > 12.5$ cm with an associated error of 0.25%.

2. The border at the junction between readout rings 7 and 8 of the masked calorimeter (C). In the standard analysis the selection criterion is $R_C < 31.25$ cm, also with an associated error of 0.25%.

To be included in the acceptance correction measurements, events had to satisfy *all the selection criteria* of the standard luminosity analysis, with the exception of the acceptance requirement being studied, and have one and only one fired strip inside the signal window in each plane. The strip in plane 1 had to overlap in Φ with the strip in plane 3 and the miss-distance with respect to the interaction point of the reconstructed track was required to be less than three times the standard deviation.

4.1.1 Inner radius

This acceptance border must be well inside the active area of the tracker to allow all events in the class $\overline{T}$ to be measured. In addition, the acceptance border must be at a lower equivalent radius than the ring mask ($r = 13$ cm at $z = 231.8$ cm), in order that the ring always acts as the primary acceptance border for all movements and offsets of the interaction point position away from the symmetry axis of the ring *and for possible* tilts of the beam axis. From these considerations, the acceptance border in the tracker was chosen to be $R_{tracker} > 12.05$ cm at a z position equivalent to the mean position of plane 1 ($z = -230.0$ cm).

The next step was to identify a radial acceptance border in the calorimeter which minimized the correction. In figures 16 and 17, the distributions of R_{cal} for the events with tracker $R_{tracker}$ below the tracker acceptance (solid histogram) and within the tracker acceptance (dotted histogram) for tracker planes 1 and 3, respectively, are shown. Both plots reveal a small, symmetric overlap region. For both planes the symmetry point is roughly at $R_A^{sym} = 12.82$ cm, and this value was chosen as the calorimeter acceptance border.

The integrated luminosity measured by the calorimeter on the full data sample is $L = N(1 + C)/\sigma$, where σ is the visible cross section, C the relative correction to the calorimeter's acceptance measured with the tracker and N the number of

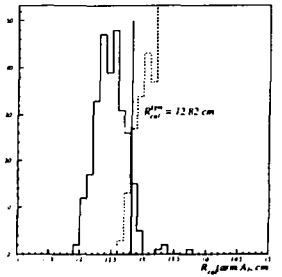

Figure 16: Distributions of unmasked calorimeter (arm A) reconstructed shower radius (R_{cal}) for the cases of fired tracker strip in plane 1 below inner residual radius tracker cut (solid line) and above cut (dashed line).

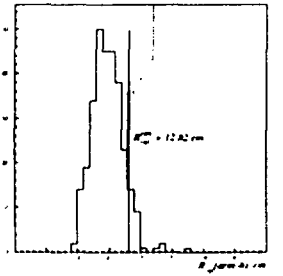

Figure 17: Distributions of unmasked calorimeter (arm A) reconstructed shower radius (R_{cal}) for the cases of fired tracker strip in plane 3 below inner residual radius tracker cut (solid line) and above ... dashed line)

Case	R_{TRK} (cm)	Plane	R_{CAL} (cm)	N_C	$N_{\bar{C}}$	$N_{\bar{C}T}$	n_{MC}	N_{data}	$\Delta L/L$ (%)
I	12.05	1	12.82	28829	18	17	299145	188163	-
II	12.05	3	12.82	30018	21	28	299131	188163	-0.03± 0.03
III	12.15	1	12.91	28791	23	24	298729	187916	-0.01± 0.03

Table 3: Results of the study of the inner radial acceptance border in calorimeter A. The visible cross-section is proportional to the number of events within the acceptance of the tracker measured with the detector simulation, n_{MC}, and N_{data} is the number of events within the calorimeter acceptance in the full data sample. The last column shows the relative difference between the given luminosity measurement and that of case I.

accepted Bhabha events in the calorimeter. The difference in the luminosities measured with two different acceptances can be written

$$\Delta L/L = (L_1 - L_2)/L_1 = 1 - \frac{N_2}{N_1}\frac{(1+C_2)}{(1+C_1)}\frac{\sigma_1}{\sigma_2}, \qquad (2)$$

where *subscripts* 1 and 2 indicate the different acceptances. The visible cross section ratio σ_1/σ_2 was computed with samples of one million Bhabha scattering events generated with the BABAMC [14] Monte Carlo program. The acceptances were simulated by making cuts on the generated 4-vectors and these partially simulated acceptances were corrected by the changes to the acceptances observed when applying them to a smaller set of events which had been processed through the full detector simulation as well. This method reduces the statistical errors in both relative and absolute luminosity measurements to a minimum for a given sample of fully simulated events.

Table 3 shows the results of three different measurements of the luminosity with all the cuts from the standard luminosity measurement except the acceptance border at the inner radius opposite the lead ring. The visible cross-section ratio σ_1/σ_2 is equal to n_1/n_2. The three measurements are consistent within their statistical errors, which are typically ±0.02%.

4.1.2 Outer radius

The outer radius of the tracker acceptance region was chosen to maximize the number of selected Bhabha events while insuring that the entire event class CT was measured. The optimal acceptance of $R_{track} < 26.35$ cm at a z position equivalent to the mean position of plane 1 ($z = -230.0$ cm) was chosen. Figures 18 and 19 show the distributions of radial positions measured by the calorimeter when the tracker cuts in planes 1 and 3 were satisfied (solid line) or not (dashed line)

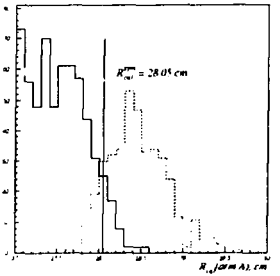

Figure 16: Distributions of unmasked calorimeter (arm A) reconstructed shower radius (R_{cal}) for the cases of fired tracker strip in plane 1 below outer radius tracker cut (solid line) and above cut (dashed line).

The stability of the luminosity with respect to changes in the acceptance definition was tested by measuring the luminosity for 4 different acceptances defined in plane 1 and for one acceptance defined in plane 3 (the radius in the table is projected to the equivalent radius in plane 1). The results are summarized in table 1 and the 5 measurements are consistent within 0.03%.

The stability of the luminosity measurement was also checked by varying the cut on the radial position measured by the calorimeter around the point which minimized the correction C. Contrary to expectations, it was discovered that the results were strongly dependent on the choice of calorimeter radius cut. In addition, it was discovered that the efficiency of the tracker had a significant radial dependence, as shown in figure 20. The data used in the measurement of the correction factor C were subsequently corrected by a *polynomial fit* to the observed relative efficiency. The corrected number of accepted events is shown in figure 22 for a range of cuts on the calorimeter radius around the point which minimizes the correction C for the 4 acceptances in plane 1 used in table 1. The average of the absolute values of the differences in luminosity between the 4 points where the correction is minimized and the nearby points is 0.01%. Figure 22 and table 1 also show that the radial dependence of the efficiency can be neglected if the calorimeter acceptance is chosen to minimize the acceptance correction. Thus the inner residual cut is not affected by the radial efficiency dependence.

The large dips in the efficiency at approximately R = 14.7, 19.2 and 23.9 cm (regions of radial overlap) are due to the suppression of events with more than

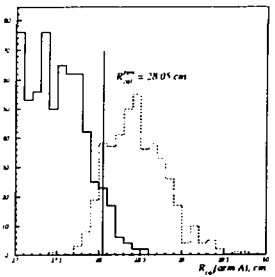

Figure 19: Distributions of unmasked calorimeter (arm A) reconstructed shower radius (R_{cal}) for the cases of fired tracker strip in plane 3 below outer radius tracker cut (solid line) and above cut (dashed line).

Case	R_{TRK} (cm)	Plane	R_{CAL} (cm)	N_C	$N_{C\bar{T}}$	$N_{\bar{C}T}$	n_{MC}	N_{data}	$\Delta L/L$ (%)
IV	26.35	1	28.05	28607	44	46	280997	178121	
V	26.35	3	28.05	29783	46	44	280997	178121	0.01 ± 0.05
VI	26.15	1	27.80	28480	48	50	279572	177226	0.00 ± 0.05
VII	25.15	1	26.81	27857	61	56	272160	172518	0.03 ± 0.07
VIII	24.55	1	26.16	27456	40	43	267195	169351	0.01 ± 0.08

Table 4: Results from the study of the outer radial cut. N_C is the number of events in the measurement of the relative correction C within the calorimeter acceptance, n_{MC} is the number of Monte Carlo events within the tracker acceptance, and N_{data} is the uncorrected number of accepted events within the calorimeter acceptance. The last column shows the relative differences between the first luminosity measurement and the others in the table.

Case	R_{TRK} (cm)	Plane	N_{data}	n_{MC}	Correction factor η	Comparison standard vs new $\Delta L/L$ (%)
IV	26.35	1	177301	281343	1.00006	-0.11
V	26.35	3	177301	281328	1.00018	-0.13
VI	26.15	1	176406	279917	1.00006	-0.12
VII	25.15	1	171698	272503	0.99975	-0.06
VIII	24.55	1	168531	267537	1.00010	-0.08

Table 5: Relative differences in the luminosity between the standard and the new analysis. The inner tracker cut is at 12.05 cm in plane 1 for all cases.

one hit per plane in the signal window. The discrepancy between data and Monte Carlo in the vicinity of the shadow of the edge of the lead ring at approximately R =13 cm is sensitive to the radial offset of the lead ring with respect to the tracker and to the longitudinal spread of the interaction point. The radial offset of the tracker relative to the lead ring leads to a nonuniform Φ distribution of the Bhabha events in the region of the discrepancy as seen in figure 21. The remaining discrepancy is not understood but since the tuning of the relative position of the mask and the spread of the interaction point had no effect on the visible cross-section while reducing the discrepancy itself by a factor 10, the remaining discrepancy is not expected to contribute significantly to the uncertainty in the luminosity.

4.2 Luminosity measurement.

The luminosity measurement described here differs from the standard analysis in two ways:

1. **Monte Carlo:** The residual inner and outer radial cuts are made with the electron track in arm A using tracker plane 1: 12.05 cm $< R_1^{track} <$ 26.35 cm.

2. **Data:** The residual inner and the outer radial cuts in the calorimeter are $R_A > 12.82$ cm and $R_A < 28.05$ cm, respectively. The number of accepted events is then corrected by the factor $\eta = 1 + C_{inner} + C_{outer}$.

The relative difference between the standard and the new luminosity measurements can be written as

$$\Delta L/L = 1 - \frac{N_{data}(new) \cdot \eta}{N_{data}(standard)} \frac{n_{MC}(standard)}{n_{MC}(new)}. \qquad (3)$$

where $n_{MC}(standard)/n_{MC}(new)$ is equal to the ratio of visible cross sections of the standard and new acceptances. The numbers of accepted events in the

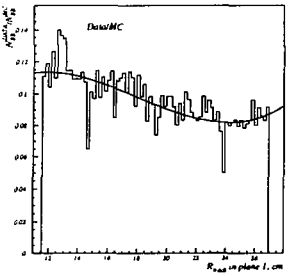

Figure 20: Ratio of number of Bhabha events in the data with good tracking information to the Monte Carlo versus the measured impact radius in plane 1. This ratio is proportional to the detection efficiency of the tracker. The curve is the result of a polynomial fit to the relative efficiency.

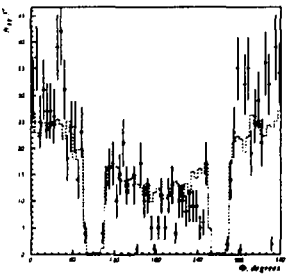

Figure 21: Number of Bhabha events versus Φ in the shadow of the lead mask in arm A ($12.45 < R_1 < 12.95$ cm at $z = -230.0$ cm). The points with solid error bars are data and the dashed line is the Monte Carlo after displacing the lead ring 1 mm along the x-axis.

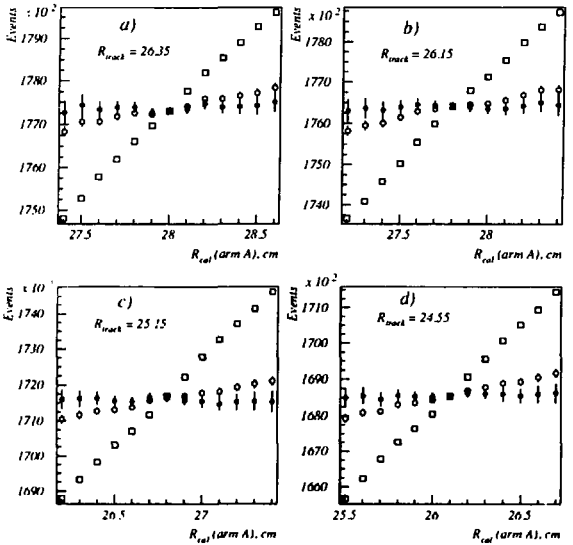

Figure 22: Corrected number of accepted events for four different acceptances defined by the tracker. The open squares show the raw numbers of accepted events versus the corresponding cut in the calorimeter. The open circles show the corrected numbers of accepted events for a given acceptance definition in the tracker. The filled circles show the same thing after taking into account the radial dependence of the detection efficiency of the tracker. Plots a), b), c) and d) show these results for tracker acceptances $R_t < 26.35$, 26.15, 25.15 and 24.55 cm, respectively.

Calorimeter R outer cut (cm)	N_{data}	n_{MC}	$\Delta L/L$ %
28.00	176811	280687	-0.07
27.75	175881	279108	-0.10
27.00	172416	273959	+0.03
26.75	171057	272016	+0.11
26.00	167476	266170	+0.05
25.75	166412	264077	-0.10
25.00	162331	257604	-0.10

Table 6: Relative difference in luminosity between the standard luminosity measurement and an alternate measurement based on corrections to the calorimeter position measurement. The residual outer radius cut in the calorimeter is varied across readout ring 6 (R_1 = 25.00 to 28.00 cm) while holding the residual inner radius cut fixed at 12.94 cm. The statistical errors on $\Delta L/L$ are typically 0.08%.

standard measurement are n_{MC} = 298928 and N_{data} = 188179. The results of five comparisons between the new and standard luminosity measurements are summarized in table 5. The results are centered around a difference of -0.10% within a range of about ±0.03%.

An alternate method to correct the calorimeter acceptance has also been tested. A fit to the average radius measured by the calorimeter versus the radius measured by the tracker in events with exactly 1 fired strip in the signal window of each plane is used to correct the position measurements of the calorimeter in the full data sample. Table 6 shows the differences between the standard luminosity measurement and this alternate measurement for seven different acceptances defined by the (corrected) calorimeter. The range of differences is about ±0.1%, which is somewhat larger than the statistical error of ~ 0.03% on the comparison.

4.3 Uncertainty

The systematic error on the luminosity due to the two radial cuts based on the tracker geometry has two main sources. The statistical uncertainties in the determinations of the correction factors contribute 0.02% and 0.03% due to the inner and outer residual cuts, respectively. The RMS spread of individual detector positions around their nominal positions is estimated from a partial survey of the detector positions to be 0.13 mm. Due to the large number of detector chips, the bias introduced to the luminosity is negligible. The dominating source of geometrical uncertainty is the precision with which the two half barrels of the tracker are fixed to each other during the mounting procedure. Due to the difficulty experienced during the mounting procedure, the lack of control of the separation of the half barrels when the mounting is completed, and from the

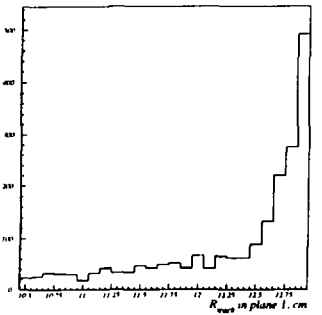

Figure 23: R (in tracker plane 1) distribution at small radii.

experience gained during *mounting tests performed outside of* DELPHI *after the* 1991 data-taking was completed, we estimate that the separation of the half-barrels could be as large as 0.8 mm. The uncertainty was taken as 1/3 of the maximum feasible separation.

Figure 23 shows that the distribution of R_1^{track} in the region of the cut at 12.05 cm is nearly uniform and contains 44 events/mm. With 37197 events in total, this corresponds to an uncertainty of $\delta L/L$=0.12%/mm. For the cut at the outer radius the uncertainty is slightly larger ($\delta L/l$ =0.20%/mm) and is anti-correlated with the cut at the inner radius. Taking into account the $\sin\Phi$ reduction of the effect of the half-barrel separation, the total geometrical uncertainty is $0.8/2/3\ mm \times 0.57 \times 0.08\%/mm$ or 0.01%.

The stability of the new method compared to the standard analysis as shown in table 5 was used to estimate an additional uncertainty of 0.03% due to the remaining effects of the non-uniform efficiency. The quadratic sum of the uncertainties discussed above is thus 0.05%.

5 Conclusions

The performance of the silicon tracker part of the DELPHI Small Angle Tagger during 1991 has been studied in detail. After taking into account the $\sim$ 5% inactive area of the tracker, efficiencies of 97 and 91% were achieved in planes 1

and 3, respectively. The average random hit probability was found to be $2 \cdot 10^{-5}$ per strip per event. This was achieved by downscaling the sampling rate of the tracker to every fourth or fifth beam crossing (22 μs per crossing) and by suppressing the noisy channels (0.8% of the total number of channels).

The tracker was then used to measure corrections to the acceptance of the calorimeter for the luminosity measurement. The final result is a correction to the standard luminosity measurement of $+0.10 \pm 0.05\%$. The uncertainty of 0.05% replaces a previous uncertainty of 0.35% [15] when the residual radial acceptance cuts were made with only the calorimeter. This work has resulted in a reduction of the total experimental systematic error on the luminosity measurement for the 1991 data from 0.6% to 0.5% [1] and removed one of the major obstacles to performing luminosity measurements with the SAT at the 0.4% level or below.

Acknowledgements

This work was supported by a grant from the Norwegian Research Council (Norges forskningsrad).

A Polynomial fit

A polynomial approach has been used to unfold the S-curve, in both the R and Φ coordinates. In the R case a spline-fit of the form:

$$F(r) = \begin{cases} 0.4633 + 0.1967r - 0.2190r^2 - 0.04307r^3 & \text{for } r \leq \text{-0.48 cm} \\ 0.1557 - 1.278r - 1.888r^2 + 2.297r^3 & \\ +6.981r^4 + 5.866r^5 + 1.730r^6 & \text{for -0.48 cm} < r < 0.11 \text{ cm} \\ 0.3364 - 4.235r + 12.81r^2 - 23.97r^3 & \\ +25.98r^4 - 14.43r^5 + 3.168r^6 & \text{for } 0.11 \text{ cm} \leq r < 0.84 \text{ cm} \\ -0.6254 + 0.2958r & \text{for } r \geq 0.84 \text{ cm} \end{cases} \quad (4)$$

has been used. The fit applies to calorimeter elements with a radial length of 3.00 cm.

The correction in Φ for calorimeter elements with an azimuthal width of 15° is:

$$F_{(1)}(\Phi) = 0.3949 - 1.169\Phi - (0.4927 \cdot 10^{-2})\Phi^2 + (0.3715 \cdot 10^{-1})\Phi^3 + (0.4498 \cdot 10^{-3})\Phi^4 - (0.2921 \cdot 10^{-3})\Phi^5 - (0.8831 \cdot 10^{-5})\Phi^6 \quad (5)$$

$$F_{(2)}(\Phi) = -0.2128 - 0.2865\Phi + (0.7402 \cdot 10^{-1})\Phi^2 + (0.1628 \cdot 10^{-1})\Phi^3 - (0.4784 \cdot 10^{-2})\Phi^4 - (0.2400 \cdot 10^{-3})\Phi^5 + (0.7624 \cdot 10^{-4})\Phi^6 \quad (6)$$

for $(-4.00° \leq \Phi \leq 4.00°)$.

After the correction using equation (5), a new fit, equation (6), is applied. The calorimeter elements with a sector opening of 7.5 degrees and a radial extension of 3.00 cm have also been treated by the latter procedure with:

$$F_{(1)}^{(7.5)}(\Phi) = 0.3186 - 0.2555\Phi - (0.3882 \cdot 10^{-1})\Phi^2 \quad (7)$$

$$F_{(2)}^{(7.5)}(\Phi) = -0.1221 - 0.1356\Phi + (0.5601 \cdot 10^{-2})\Phi^2. \quad (8)$$

B Dead Balder chips

The Balder chips which are observed to be dead during 1991 are listed in table 7. They constitute about 5% of the total detector area.

Plane 1		Plane 3	
Block	Balder	Block	Balder
1	36	0	22
1	37	1	17
1	38	1	62
1	39	4	0
3	0	5	16
3	1	5	17
3	2	5	18
3	3	5	28
3	22	5	29
3	41	5	30
4	20		
4	21		
4	22		
4	23		
5	26		

Table 7: Dead Balder-chips.

References

[1] P.Abreu et al. (DELPHI collaboration), *Measurements of the Lineshape of the Z^0 and Determination of Electroweak Parameters from its Hadronic and Leptonic Decays*, DELPHI draft 0073, version 2. To be submitted to Nuclear Physics **B**.

[2] DELPHI-collaboration. *The DELPHI detector at LEP.* Nucl. Inst. and Meth. **A303** (1991) 233-276

[3] L. Bugge et al. *DELPHI SAT Luminosity Analysis: 1990.* DELPHI 91-104 PHYS-147. November 1991.

[4] E. Nygaard et al. *"Balder" - a 48 Channel Front-end Circuit in CMOS for Silicon Detectors - User's Guide.* Senter for Industriforskning (SI) internal report, Oslo, 1989.

[5] T. Buran et al. *The SAT tracker in DELPHI. A technical description.* Under preparation.

[6] A K Topphol. *The SAT Calorimeter. An Analysis of its Performance* Dr. Scient. thesis, Department of Physics, University of Bergen, January 1990

[7] W. R. Nelson, H. Hirayama, and D. O. Rogers. *The EGS4 Code System.* SLAC-Report-265, December 1985.

[8] E. Wilhelmsen. *A study of the tracker data and the data readout system for the Small Angle Tagger in the DELPHI experiment at LEP.* Master's thesis, Department of Physics, University of Oslo, May 1991.

[9] A. D. Christoffersen. *A study of position reconstruction in the Small Angle Tagger Calorimeter and a study of beam- and luminosity monitoring in the Very Small Angle Region in the DELPHI experiment.* Master's thesis, Department of Physics, University of Oslo, 1990.

[10] T. Seland. *A study of the Electromagnetic shower development in the SAT/DELPHI detector at LEP using EGS4.* Master's thesis, Department of physics, University of Oslo, November 1991.

[11] M. Dam. *Bhabha Scattering Detected by a Small Angle Tagger as a Luminosity Monitor for the DELPHI Experiment at LEP.* Master's thesis, Department of Physics, University of Oslo, 1987.

[12] L. Bugge, Nucl.Instr.and Meth.**A242**(1986)228.
G. A. Akopdjanov et al., Nucl.Instr.and Meth.**140**(1977)441.

[13] L. Bugge et al. *Preliminary SAT Luminosity Analysis: 1991.* DELPHI 91-81 CAL81 PHYS-147. August 1991.

[14] M.Böhm, R.Kleiss, and W.Hollik, Nucl.Phys.**B304**(1988)712.

[15] P.Abreu et al. (DELPHI collaboration), Nucl.Phys.**B367**(1991)511.

FYSISK INSTITUTT
FORSKNINGS-GRUPPER

DEPARTMENT OF PHYSICS
RESEARCH SECTIONS

Biofysikk	Biophysics
Elektronikk	Electronics
Elementærpartikkelfysikk	Experimental Elementary Particle Physics
Faste stoffers fysikk	Condensed Matter Physics
Kjerne- og energifysikk	Nuclear and Energy Physics
Plasma- og romfysikk	Plasma and Space Physics
Strukturfysikk	Structural Physics
Teoretisk fysikk	Theoretical Physics

ISSN 0332-5571